Multiple-component lattice Boltzmann equation for fluid-filled vesicles in flow

I. Halliday*
Materials and Engineering Research Institute, Sheffield Hallam University, Sheffield, S1 1WB, UK

S. V. Lishchuk
Department of Mathematics, University of Leicester, Leicester, LE1 7RH, UK

T. J. Spencer
Materials and Engineering Research Institute, Sheffield Hallam University, Sheffield, S1 1WB, UK

G. Pontrelli
IAC-CNR Roma, Via dei Taurini 19, 00185 Roma, Rome, Italy

C. M. Care
Materials and Engineering Research Institute, Sheffield Hallam University, Howard Street, S1 1WB, UK
(Received 18 July 2012; revised manuscript received 14 January 2013; published 22 February 2013)

We document the derivation and implementation of extensions to a two-dimensional, multicomponent lattice Boltzmann equation model, with Laplace law interfacial tension. The extended model behaves in such a way that the boundary between its immiscible drop and embedding fluid components can be shown to describe a vesicle of constant volume bounded by a membrane with conserved length, specified interface compressibility, bending rigidity, preferred curvature, and interfacial tension. We describe how to apply this result to several, independent vesicles. The extended scheme is completely Eulerian, and it represents a two-way coupled vesicle membrane and flow within a single framework. Unlike previous methods, our approach dispenses entirely with the need explicitly to track the membrane, or boundary, and makes no use whatsoever of computationally expensive and intricate interface tracking and remeshing. Validation data are presented, which demonstrate the utility of the method in the simulation of the flow of high volume fraction suspensions of deformable objects.

DOI: 10.1103/PhysRevE.87.023307 PACS number(s): 47.11.−j

I. INTRODUCTION

The flow of incompressible fluids containing a large volume fraction of deformable particles, or vesicles, is a fundamental matter which impacts upon *inter alia* the microscale flow of blood in vessels of diameter $<100\,\mu$m, where it (blood) cannot be considered a continuum.

Secomb and Pries and their coworkers have worked extensively on flows containing single red blood cells, vesicles, and capsules. These authors have developed a range of analyses and computational models, based upon traditional numerical techniques, which address problems ranging from the physics of individual vesicles in flow (see Skotheim and Secomb [1] and the references therein) to careful models of single red blood cells flowing along microcapillaries with complex boundary shapes and interactions (see, e.g., Secomb *et al*. [2] and the references therein).

Other previous work is more closely related to ours here, which is based upon hydrokinetic methods. Using a boundary integral technique to represent a single membrane-enclosed vesicle in flow, Kaoui and his coworkers have considered fundamental questions of red blood cell shape asymmetry [3] and computed the migration of a single, deformable bicuspid vesicle in an unbounded shear flow [4]. The latter approach was combined, with a hydrokinetic or lattice Boltzmann equation (LBM) flow solver, to simulate tank-treading motion under confined shear [5]. Similar "immersed-boundary" techniques [6] were combined with LBM by Zhang *et al*. to address the problem of up to four, deformable capsules in two dimensions [7] and recently by Krüger *et al*. [8], who assess very carefully the accuracy of the general method.

In practical terms, the work of Dupin *et al*. [9] is a benchmark. Dupin was the first to address the high concentration, fully three-dimensional (3D) regime, using LBM-based methods, successfully simulating of the order of a hundred red blood cells, flowing in cylindrical, large-capillary scale confined geometry. While Dupin *et al*. pointed a way to simulations of blood at this scale, with moderate numbers of explicitly resolved, deforming cells, their approach was not without limitations. The demonstrability of the physical boundary conditions at the vesicle surface, control of ballistic impact between vesicles and the algorithmic complexity, necessary to convect and deform 3D vesicles, using a separate surface mesh of points and facets for every vesicle, represent important limitations. Possibly the most important recent innovation in the explicit simulation of blood is due to Melchionna *et al*., who devised an LBM-based simulation which retains a carefully calculated, minimal, but still explicit representation of rigid red blood cells and can, as a consequence, access cardiovascular scales [10,11].

The studies identified above already incorporate all the membrane physics included in the present work, though by use of very different methods and with different degrees of verifiability. The present work is an advance in

*i.halliday@shu.ac.uk

technique; its objective is to provide an analytically verifiable, single-framework methodology, for the accurate simulation of multiple vesicle systems, with an accessible algorithm and access to a scaling of computation which is predictable and efficient, as both the number of vesicles and the dimensionality of the problem are increased [12]. To this end, we consider how to embed a similar concept of a membrane (and, hence, vesicle) into a different class of LBM simulation, the multicomponent lattice Boltzmann (MCLB) method.

The list of areas in which LBM [13–15] has advantages over traditional computational fluid dynamics is of restricted length. Computation of the flow of immiscible, interacting fluid components is, however, close to its top. In this article, we extend an MCLB technique for multiple immiscible fluids, described in the isothermal, continuum regime of arrested coalescence, generalizing the extant method of maintaining an interface between separated fluids to allow one to model the physical properties of a closed membrane of given interfacial tension, bending rigidity, and interface compressibility, while conserving enclosed volume and membrane area.

There are excellent reasons to found the simulation of multiple, discrete vesicles upon MCLB simulation: (1) vesicle volume is automatically conserved, since the internal fluid is incompressible, (2) MCLB techniques with arrested coalescence and appropriate interface kinematics (free from unphysical cross-interfacial fluxes) already exist, (3) MCLB techniques with efficient representation of many mutually immiscible phases already exist [12,16,17], and (4) simulation of many vesicle systems requires the parallelization, by domain decomposition, to which MCLB is well adapted. Hence, we will augment an appropriately chosen MCLB algorithm, with the intention of adding to its existing Laplace law interfacial tension property, those additional properties listed above. By selecting an appropriate MCLB, vesicles' volume conservation and mutual immiscibility will accrue automatically, making for efficient multiple vesicle simulations.

We begin by setting out the assumptions implicit in our approach. Next we derive an appropriate membrane force density. We then proceed to a review of one particular, existing MCLB simulation for completely immiscible fluids separated by an interface with only Laplace law interfacial tension, then show how the immersed boundary force density in such a simulation may be straightforwardly modified, to include bending rigidity and conserved area effects. We will then consider the extension of this method to more than two mutually immiscible fluids, i.e., to multiple vesicles. Finally, we present simulation data and conclusions. For clarity, mathematical detail is placed in the Appendix, where we will also state the model extension to three dimensions, reserving detail for later publications. For simplicity we work in two dimensions throughout the majority of this work.

II. PHYSICAL AND MODELING ASSUMPTIONS

It is important to distinguish between, on one hand, the algorithmic details of the way in which an appropriate membrane boundary is created in MCLB simulation, and, on the other, the physical system which we attempt to approximate and its mathematical encapsulation. In this section, we are concerned with the latter.

Since we address a vesicle membrane within the continuum approximation of fluid mechanics, the membrane has no resolved internal structure: It is manifest as a boundary condition, controlling the interaction between two otherwise independent, incompressible flows. Put another way, any structure is an accidental artifact of our approach. We also assume that the membrane is impermeable, with a negligible flux of fluid across it. The membrane we consider is similar to that considered by Kaoui *et al*. [4]. Physically, such a membrane is a phospholipid bilayer which may be viewed as a 2D incompressible fluid. Hence, any flow of the membrane must be everywhere in the direction of its local tangent plane. We pursue this matter in detail in the Appendix.

We suppose that the microscale properties of the membrane allow local strains to relax very rapidly, relative to time scales characteristic of the continuum regime of viscous flow, in which regime both the separated fluids and the membrane faces must move at the same speed, locally. The boundary conditions on the flow may therefore be stated as a requirement that the separated, immiscible fluids and the interface, or membrane, should move together (velocities would still need to match if the components were partially miscible; in the present case, however, the diffusive current also vanishes). The kinematic condition of mutual impenetrability is the requirement that the velocity of the separated fluids must match at the boundary. We consider the extent to which our method meets this requirement in the Appendix. We note that, to recover, e.g., tank-treading behavior in the vesicle, the interface, or membrane, must be able to move in the direction parallel to its local tangent plane, which is consistent with the kinematic condition of mutual impenetrability.

We shall assume that the reader is familiar with the lattice Boltzmann method [13], and we will discuss only the most relevant aspects of our core method in this article.

In summary, the final motion of the local membrane, from which tank-treading, shape deformation, and lubrication effects must all emerge, will rely on the membrane's ability to move in a manner consistent with (1) the kinematic conditions of mutual impenetrability and (2) any membrane strains accompanying the relaxation of local stresses. The treatment in the Appendix proves that requirement (1) is present in our model. The same analysis shows that negligible unphysical fluid fluxes cross the membrane. In respect of (2), recall that the present work contains an assumption of rapid relaxation of interfacial strains; i.e., we model a membrane which is always close to mechanical equilibrium where it is highly incompressible.

III. A MEMBRANE FORCE

Let us consider a plane, 2D vesicle, enclosed by a membrane represented by a closed, two-dimensional curve. That is, we describe the membrane location with a continuous, 2D regularly parameterized curve $\gamma(t) : I \to R^2$ with traditional parameter t, which corresponds to distance measured along the *undeformed* membrane. No confusion should arise from this notation, as time does not appear as a variable outside the Appendix. We denote by s the distance measured along the strained membrane.

Denote by $\mathbf{F}(\mathbf{r})$ that external force density which it is necessary to impress in an MCLB fluid, to portray the membrane. To be consistent with previous work [18] this force, arising from the membrane length element, must eventually be applied as a force density, throughout a local volume element of LBM fluid. A given volume element of fluid will be subject to both viscous and membrane forces. The former appear automatically in MCLB, but the membrane force density must be imposed as that external, immersed boundary force density which we begin to consider here.

A. Analysis of a 2D vesicle

The analysis of this section considers a single vesicle and assumes that stresses in the membrane relax quickly.

The equilibrium shape of a neutrally buoyant vesicle at rest may be obtained by constrained minimization of its excess free energy functional, subject to constraints of constant surface area and constant enclosed volume [19]. For our model, we choose to approach the constraint of constant surface area by introducing a force contribution and conservation of the volume enclosed by the membrane is automatically fulfilled (because the vesicle's interior is incompressible)and need not be considered explicitly.

Let us determine the net force acting on a length element of an isolated, 2D membrane, by forming the variational derivative of a convenient excess free energy functional, $A[\mathbf{r}(t)]$. The position of a point on the deformed membrane is

$$\mathbf{r}(t) = (x(t), y(t)), \tag{1}$$

and the local arc length is

$$ds = \sqrt{\dot{x}(t)^2 + \dot{y}(t)^2}\, dt \equiv u(\dot{x}, \dot{y})\, dt, \tag{2}$$

in which we note that $u(\dot{x}, \dot{y})$ has no explicit t dependence. It follows that the membrane length in the strained state

$$L = \int_0^{L_0} u(\dot{x}, \dot{y})\, dt, \tag{3}$$

where we denote by L_0 the unstrained length at mechanical equilibrium.

It is natural to consider a set of physically distinct contributions to the excess free energy. If the membrane is stretched from its original length, its free energy increases. The associated excess free energy is

$$A_L[\mathbf{r}(t)] = \frac{\alpha}{2} \int_0^{L_0} [u(\dot{x}, \dot{y}) - 1]^2 dt, \tag{4}$$

in which α is the membrane compressibility. The free energy arising from the membrane's departure from its preferred curvature, K_0, is

$$A_K[\mathbf{r}(t)] = \frac{\kappa}{2} \int_0^{L_0} [K(\dot{x}, \dot{y}, \ddot{x}, \ddot{y}) - K_0]^2 u(\dot{x}, \dot{y})\, dt, \tag{5}$$

where κ is the membrane bending rigidity. Note that the integrand depends upon second derivatives of $x(t)$ with respect to t. Finally, the contribution from the interfacial tension of the membrane is

$$A_S[\mathbf{r}(t)] = \sigma \int_0^{L_0} u(\dot{x}, \dot{y})\, dt, \tag{6}$$

where σ is the membrane's interfacial tension parameter. Here, the vesicle interior fluid is assumed to be incompressible, so no volume changes can occur. However, for completeness, the excess free energy associated with 2D volume (i.e., area) changes may be evaluated as follows. If the vesicle has initial volume V_0 and is assumed to be filled by a medium with compressibility C, the excess pressure is $p = C\{V[\mathbf{r}(t)]/V_0 - 1\}$, where the functional $V[\mathbf{r}(t)] = \int_0^{L_0} y(t)\dot{x}(t)\, dt$: The excess free energy due to compressibility is then $A_V[\mathbf{r}(t)] = \int_{V_0}^{V} p\, dV$.

When the vesicle volume is constant, the excess free energy may be expressed without this contribution as the following functional:

$$A[\mathbf{r}(t)] = A_L[\mathbf{r}(t)] + A_S[\mathbf{r}(t)] + A_K[\mathbf{r}(t)]. \tag{7}$$

The incremental force, $\mathbf{F}dt$, acting upon a membrane length element of length ds may be now obtained from the variational derivative of Eq. (7):

$$\mathbf{F}(t) = -\frac{\delta A[\mathbf{r}(t)]}{\delta \mathbf{r}(t)} \equiv \mathbf{F}_L(t) + \mathbf{F}_S(t) + \mathbf{F}_K(t), \tag{8}$$

with $\mathbf{F}_L(t) \equiv -\frac{\delta A_L[\mathbf{r}(t)]}{\delta \mathbf{r}(t)}$, etc. Using our stated assumptions, we show in detail in the Appendix that

$$\mathbf{F}_L(t) = \alpha \frac{L}{L_0}\left(1 - \frac{L}{L_0}\right) K \hat{\mathbf{n}}, \tag{9}$$

$$\mathbf{F}_S(t) = -\sigma \frac{L}{L_0} K \hat{\mathbf{n}}, \tag{10}$$

$$\mathbf{F}_K(t) = \kappa \frac{L}{L_0}\left[\frac{1}{2}K\left(K^2 - K_0^2\right) + \frac{d^2K}{ds^2}\right]\hat{\mathbf{n}}, \tag{11}$$

where $\hat{\mathbf{n}}$ is positive in the direction pointing away from the volume enclosed by the membrane. Despite its composite character, the net force on length element, ds, is apparently directed purely in the surface-normal direction, which assists the stability of the method. The above expressions are similar to and consistent with those derived by Kaoui *et al.* [4].

It is appropriate to recall that we have derived, in this subsection, a force per unit length of membrane. It is necessary to convert this force to a suitable force density.

B. Application to MCLB simulation

How is the membrane physics of the previous section to be incorporated into a MCLB simulation? The most accessible MCLB interface is that due to Lishchuk *et al.* [20]. We consider first how to adapt Lishchuk's method to the simulation of single vesicles. Subsequently, we will present an extension to multiple vesicles. We will consider the extent to which other MCLB interface methodologies (e.g., the popular Shan-Chen method [21]) might be utilized in our discussion.

Since the pioneering work of Gunstensen and Rothman [22], several two-component MCLB methods have arisen. Each is distinguished by the way in which it imposes an interface. Where the kinematics of phase separation must be considered, *free-energy* methods [23,24] and their thermodynamically consistent extensions, due to Wagner and coworkers [25–27], based, as they are, on the Cahn-Hilliard theory, are appropriate. For workers with a background in molecular simulation, the Shan-Chen method [21] is a natural choice. We use the MCLB interface of Lishchuk *et al.* [20],

which is adapted to completely arrested coalescence, i.e., completely immiscible fluids, considered in the continuum approximation. Lishchuk's method for interfacial tension [20], used with appropriate component segregation [28], furnishes a robust MCLB technique with assigned surface tension and continuum interfacial kinematics and dynamics. A further, key, advantage of MCLB methods, including Lishchuk's method, is that one can restrict computational memory requirements, such that, in two dimensions, for a number of immiscible components $M > 5$, computational memory requirements do not increase and execution time increases only slowly [16,17]. While it is not relevant here, it is important to note that generalization of Lishchuk's method to $M > 2$ mutually immiscible components requires care (if correct Laplace-Young behavior is to emerge [18]).

In Lishchuk's method, Laplace law and "no-traction" effects arise from a curvature-dependent external force density, impressed primarily in regions where the fluid components' phase field varies most rapidly. Suppose two fluid distributions which occupy lattice link i, at position $\mathbf{r}$ to be described by distribution functions, $R_i(\mathbf{r})$ and $B_i(\mathbf{r})$ [of course, with $f_i(\mathbf{r}) = R_i(\mathbf{r}) + B_i(\mathbf{r})$]. The nodal density of the red and blue fluids,

$$\rho_R(\mathbf{r}) = \sum_i R_i(\mathbf{r}), \quad \rho_B(\mathbf{r}) = \sum_i B_i(\mathbf{r}), \tag{12}$$

is used to define A local phase field [28]:

$$\rho^N(\mathbf{r}) = \frac{\rho_R(\mathbf{r}) - \rho_B(\mathbf{r})}{\rho_R(\mathbf{r}) + \rho_B(\mathbf{r})}. \tag{13}$$

Surfaces $\rho^N = \text{const}$ define the interface, and $\rho^N = 0$ is taken to be its center. Throughout the narrow but distributed interfacial region, the local interface normal is

$$\hat{\mathbf{n}} = -\frac{\nabla\rho^N}{|\nabla\rho^N|}. \tag{14}$$

With this definition, for a red drop in a blue fluid, the interface normal unit vector, $\hat{\mathbf{n}}$, points away from the enclosed red fluid. Local interfacial curvature is obtained from the surface gradient of $\hat{\mathbf{n}} = (\hat{n}_x, \hat{n}_y)$, which, in two dimensions, is [20]

$$K \equiv \hat{n}_x\hat{n}_y\left(\frac{\partial\hat{n}_y}{\partial x} + \frac{\partial\hat{n}_x}{\partial y}\right) - \hat{n}_y^2\frac{\partial\hat{n}_x}{\partial x} - \hat{n}_x^2\frac{\partial\hat{n}_y}{\partial y}. \tag{15}$$

All the derivatives in Eqs. (14) and (15) may be computed to third-order accuracy with an appropriate stencil:

$$\frac{\partial f}{\partial x_\alpha} = \frac{1}{k_2}\sum_{i\neq 0} t_i f(\mathbf{r} + \mathbf{c}_i)c_{i\alpha} + o(h^4), \tag{16}$$

where h denotes lattice spacing, the lattice isotropy constant $k_2 = c_s^2 = 1/3$ for our $D2Q9$ lattice, and the summation omits the rest link direction $i = 0$. The above stencil's convenience and accuracy arises indirectly, as a consequence of the careful way in which LBE simulation lattice geometries are chosen [13]. Clearly, the number of grid points required to calculate a gradient depends upon the cardinality of the LBE lattice unit cell's basis set, Q. To avoid misleading the reader, however, let us consider the number of grid points implicit in the calculation of second-gradient K, being a gradient of $\hat{n}$, itself a gradient in ρ^N. $Q - 1$ neighbors are visited to compute the gradient of $\hat{n}$, with each neighbors's value of $\hat{n}$ itself requiring $Q - 1$ visits, implicating a total of $(Q - 1)^2$ neighbors in the calculation of K. However, this overestimate neglects repeated visits to common neighbors. In the case of a $D2Q9$ lattice, visits may be rationalized, using a predetermined stencil (based directly upon that above) involving only 25 neighbors.

Application of the normally directed force density:

$$\mathbf{F} = \tfrac{1}{2}\nabla\rho^N\sigma K, \tag{17}$$

in which $\frac{1}{2}\nabla\rho^N$ is an appropriate weight biasing phase field boundary regions [20], may be shown to recover correct dynamics for the continuum regime [20]. That is, a Laplace law pressure step [29] across interfacial regions and the no-traction condition arise from the force density in Eq. (17).

Correct interfacial kinematics arise from an appropriate segregation step. The kinematic property of mutual impenetrability emerges from correctly chosen, postcollision color segregation rules [28]. In the Appendix, we consider the cross section of the interface (it is central to this work that phase fields have constant width, irrespective of interface orientation, relative to the lattice)

He *et al.* [30] and Guo *et al.* [31] generalized the LBGK model, originally devised by Qian *et al.* [32], to describe lattice fluid subject to a known, spatially variable external force denisty, $\mathbf{F}$. Collision and forcing of the distribution function are

$$f_i^\dagger = f_i^{(0)}(\rho,\rho\mathbf{u}) + \left(1 - \frac{1}{\tau}\right)f_i^{(1)}(\nabla\rho,\ldots,\partial_x u_y,\ldots,\mathbf{F}) + F_i(\tau,\mathbf{F},\mathbf{u}), \tag{18}$$

where the dagger superscript indicates a postcollision, prepropagate quantity, $f_i^{(0)}(\rho,\mathbf{u})$ denotes the equilibrium distribution function [13], and the source term, F_i is

$$F_i = t_i\left(1 - \frac{1}{2\tau}\right)\left[\frac{\mathbf{c}_i - \mathbf{u}}{c_s^2} + \frac{(\mathbf{c}_i\cdot\mathbf{u})(\mathbf{c}_i)}{c_s^4}\right]\cdot\mathbf{F}, \tag{19}$$

where all symbols have their usual meaning; see, e.g., Ref. [28].

Shortly, we shall write a generaliazed form of the force density in Eq. (17), which imparts membrane physics. We stress that this generalized force density can be handled without any further modification of the methodology outlined in this subsection.

C. MCLB membrane force density

To avoid unphysical transverse fluxes, the interface or membrane must advect in flow in a manner consistent with the kinematic condition of mutual impenetrability, without dispersion and without introducing significant noise in the underlying flow simulation method. The analysis in the Appendix shows that these requirements are met in our model. Further to these kinematic conditions, additional physics is required. This is obtained by generalizing the MCLB force density for "Laplace law" physics, embedded in Eq. (17), into a form which accords with the membrane force introduced in Sec. III A.

To obtain an expression for membrane force density, we transform the force acting on a length ds, $\mathbf{F}dt$, given by Eq. (8), by dividing by an expression for ds. Recall that parameter,

t, corresponds to length measured along the equilibrium membrane shape, which has length L_0. By assuming that the stresses in the strained membrane, length L, relax rapidly relative to flow time scales and that membrane strain is uniform throughout, one obtains $\frac{ds}{dt} = \frac{L}{L_0}$, or $ds = (L/L_0)dt$. Hence, using Eq. (8) and canceling factors of L/L_0, the force per unit length of membrane, or membrane force density is

$$\mathbf{F} = \frac{1}{2}\nabla\rho^N K\left[\sigma - \alpha\left(1 - \frac{L}{L_0}\right) - \frac{\kappa}{2}\left(K^2 - K_0^2\right)\right] - \frac{\kappa}{2}\nabla\rho^N\frac{d^2K}{ds^2}, \tag{20}$$

The assumptions we have made results in this expression, which is particularly convenient for computation. Note that the phase field gradient $\frac{1}{2}\nabla\rho^N$, which is introduced as a weight, is positive in the direction of $-\hat{\mathbf{n}}$, the factor $1/2$ being necessary to produce the correct cumulative force, since $\int_{-\Delta}^{\Delta}\frac{d\rho^N}{dx}dx = \rho^N(\Delta) - \rho^N(-\Delta) = 2$ (here, $\pm\Delta$ are locations deep within the blue and red fluids, where $\rho^N = \pm 1$). Also note that in the distributed force density of Eq. (20), $K = 1/R$ varies with position. Let us estimate its expectation value as follows. $\langle\frac{1}{R}\rangle = \frac{1}{2}\int_{-\Delta}^{\Delta}\frac{d\rho^N}{dx}(\frac{1}{R_0+x})dx$, in which R_0 is the radius of curvature of the $\rho^N = 0$ contour. Suppose $x/R_0 < 1$ and take a binomial expansion to $o[(x/R_0)^2]$ in the integrand. Noting that the weight $\frac{d\rho^N}{dx}$ is an even function, the term linear in x/R_0 gives an odd contribution and $\langle\frac{1}{R_0}\rangle \simeq \frac{1}{2R_0}(\int_{-\Delta}^{\Delta}\frac{d\rho^N}{dx}\,dx + \frac{2}{R_0^2}\int_0^{\Delta}\frac{d\rho^N}{dx}x^2\,dx)$. Approximating the second integral using the trapezium rule returns a value of 3.45, hence the $\langle\frac{1}{R}\rangle = \frac{1}{R_0} + \frac{3.45}{R_0^3}$. From this, it is possible to estimate the error in $K = \frac{1}{R_0}$ attending the use of the distributed force density in Eq. (20): For $R_0 > 8$, this error is less than 5%.

Let us return to the membrane force density in Eq. (20). We note that Laplace law behavior is restored by setting $\alpha = \kappa = 0$ (which then corresponds to the force density of Lishchuk's method), that a weight $\frac{1}{2}\nabla\rho^N$, introduced in place of $\hat{\mathbf{n}}$, produces a smoothly varying external force density, with the correct cumulative effect in unit length of membrane (see next section), that $\mathbf{F}$ still acts purely in the direction of the interface normal, that an effective, length-dependent surface tension:

$$\sigma'(\sigma, L, L_0, \alpha) = \sigma - \alpha\left(1 - \frac{L}{L_0}\right), \tag{21}$$

which can be negative can be considered to act, that, in comparison with a Laplace law model, the membrane force density requires only the additional calculation of interface length, L, and, finally, that the second gradient of curvature must calculated, after Eq. (15), using a surface gradient calculation:

$$\frac{dK}{ds} = \hat{n}_x\hat{n}_y\left(\frac{\partial K}{\partial x} + \frac{\partial K}{\partial y}\right) - \hat{n}_y^2\frac{\partial K}{\partial x} - \hat{n}_x^2\frac{\partial K}{\partial y}, \tag{22}$$

repeatedly. Henceforth, we set the preferred curvature, $K_0 = 0$, corresponding to a flat membrane.

The membrane force density of Eq. (20) has three steady contributions, controlled by parameters κ, α, σ, and L. Since α, σ, and L span a single effective interfacial tension, the membrane force density has only two independent parameters, σ' and κ. Moreover, the force density is always normally directed. These facts underlie the stability of the present model, but this stability will be jeopardized by extensions of the model's physical content, such as the fluid density contrasts to be discussed in Sec. III F and when resolution is inadequate accurately to compute Eq. (22) (see Sec. IV).

D. Numerical measurement of interface length and width

The membrane force density in Eq. (20) depends upon a measurement of vesicle boundary length, L. We must therefore devise an accurate, robust, efficient, and easy to implement interface length measurement which takes into account the fact that the phase field which defines the interface, ρ^N, varies in two dimensions. (In bulk fluids, ρ^N has a constant value but changes "continuously" at the interface between phases.)

Let the interface occupy region $\mathbf{r} : |\nabla\rho^N|(\mathbf{r}) < 1.0 \times 10^{-8}$. Suppose that $\hat{\mathbf{n}}\cdot\nabla\rho^N$ depends only on the scalar distance, n, measured perpendicular from the $\rho^N = 0$ contour, in the direction of $\hat{\mathbf{n}}$; i.e., suppose that $\hat{\mathbf{n}}\cdot\nabla\rho^N$ is independent of the orientation of the interface relative to the lattice. To provide a value for L, the 2D area, A_0, of the interfacial region is defined and measured, then divided by an appropriately defined interface width, W_0, measured in the direction of $\nabla\rho^N$. Clearly, it is essential that the boundary phase field has a transverse variation which is independent of orientation relative to the lattice, independent of motion relative to the lattice and allows W_0 to be considered a small, global constant. These properties are considered in the Appendix and assumed here.

Assuming the variation of the phase field is described by $\rho^N = \tanh(\beta n)$, with β the segregation parameter used in Lishchuk's method [28], convenient numerical values for A_0 and W_0 are obtained as follows. An appropriate choice of an interfacial weight function is $|\nabla\rho^N| = \beta(1 - \rho^{N2})$ [18] ($\beta = 0.67$ in this work). The lattice area, A_0, occupied by interfacial fluid is now defined as a surface integral, which is well approximated by a quadrature, or whole lattice summation:

$$A_0 \equiv \int\int\left(1 - \rho^{N2}\right)dS \simeq \sum_{\mathbf{r}}[1 - \rho^N(\mathbf{r})^2]. \tag{23}$$

This is essentially a discrete summation of $|\nabla\rho^N|$. For unit length of interface, we define a second integral, which we again approximate as a lattice summation:

$$W_0 \equiv \int\left(1 - \rho^{N2}\right)dn \simeq \sum_{\mathbf{r}\in S_0}[1 - \rho^N(\mathbf{r})^2], \tag{24}$$

in which summation the discrete values of $\mathbf{r}$ are restricted to a subset, S_0, of the lattice which corresponds to strip of unit width, orientated perpendicular to the contour $\rho^N = 0$. For a $D2Q9$ lattice [13], a numerical integration; i.e., a lattice summation yields $2.947 \leqslant W_0 \leqslant 2.985$, depending upon the orientation of the interface with respect to the lattice. W_0 is considered to be a constant. The summation in Eq. (23), however, must be evaluated at every time step, the length of the membrane interface being conveniently defined as follows:

$$L = \frac{A_0}{W_0}. \tag{25}$$

Tests of this method conducted on flat interfaces, inclined at a range of angles relative to the lattice, show the value of interfacial length obtained in this way compares well to its geometrical length, the maximum error corresponding to 4% .

The value of W_0 does not estimate the geometrical interface width. A measure of the latter is obtained by considering the distribution of the force density in Eq. (20), as follows. Consider a flat interface. The weight of the force density is $\frac{1}{2}\frac{d\rho^N}{dx}$, where x is distance perpendicular to the interface and let $\rho^N(0) = 0$. Hence $\langle x\rangle = 0$. The interface width may be estimated from $\sqrt{\langle x^2\rangle}$. $\langle x^2\rangle = \int_{-\Delta}^{\Delta} \frac{1}{2}\frac{d\rho^N}{dx} x^2 dx$. Now, weight $\frac{1}{2}\frac{d\rho^N}{dx}$ is an even function well approximated by $\beta[1-\rho^N(x)^2]$ [18] where $\beta = 0.67$ is the segregation parameter [28,33] defined in Eq. (A20). We analyze the segregation process in the Appendix. Now $\langle x^2\rangle = \int_{-\Delta}^{\Delta} \frac{1}{2}\beta(1-\rho^N x^2)x^2\, dx \approx 1.727$ using a trapezium rule approximation. Hence, the finite geometrical width of the interface may be estimated:

$$\sqrt{\langle x^2\rangle} \approx \sqrt{1.727} = 1.314 \tag{26}$$

for $\beta = 0.69$. The value of interface segregation parameter, β, would clearly affect this number. $\beta = 0.69$ is a maximum for stable operation [28] and 1.314 lattice units represents the minimum interface thickness. Moreover, any layer of fluid of thickness <1.314, being thinner than the interface must be regarded as badly resolved. We return to this point. The above value of $\sqrt{\langle x^2\rangle}$ is well supported by simulations, is independent of the interface orientation and local flow (see the Appendix), and is not influenced by any parameter other than computational resolution (considered below) except for Laplace law interfaces with large interfacial tension, when pressure (i.e., lattice fluid density [13]) varies rapidly in the interfacial region, and the assumptions made in predicting the interfacial width degrade. In the present context, the pressure step across the membrane is very small, and the width of the interface, i.e., the ρ^N variation is independent of mechanical parametrization and local flow environments. This observation is, again, supported by simulations. In Sec. IV, we shall return to assess, in context, the effect of resolution on the sharp interface behavior of the present vesicle model. Note that our model converges on a stable interfacial profile in time steps on the order of a hundred, independent of the value of β.

E. Bulk vesicle properties in MCLB

A vesicle is, in general, filled with an incompressible fluid, red fluid, which may have a significantly different viscosity from the embedding blue fluid. In principle, the internal fluid may also have a density contrast, though for our envisaged applications, the latter is likely to be small.

Our MCLB model will accommodate significant viscosity contrast satisfactorily, by continuously varying the LB collision parameter, τ, from τ_B to τ_R, with a profile which matches the phase field variation (data not shown):

$$\tau(\mathbf{r}) = \frac{\tau_R + \tau_B}{2} - \rho^N(\mathbf{r})\left(\frac{\tau_R - \tau_B}{2}\right), \tag{27}$$

but its ability to accommodate a significant density contrast is more restricted. In the past, we developed a method for simulating a density contrasts across the closely related Laplace law interface, which relies upon the action of a tangentially directed, "insulating" force, acting only in the interfacial region, to regulate the transmission of shear stresses in accord with an assumed density contrast (which is different from the LB density, ρ) [34]. In principle, this method could also be applied the the present model directly. However, the convenient structure of the membrane force density in Sec. III C, is undermined by a tangential force component, which would have destabilizing effects, certainly at low resolutions. Nevertheless, with adequate resolution, moderate effective density contrasts may be accessible to the present method, which matter we will pursue in a future publication.

F. Multiple vesicles in MCLB

Different vesicles must not coalesce, overlap or attach in flow. We describe, in this subsection, minimal modifications which adapt, to the case of many vesicles, one MCLB technique [18] for $M \gg 2$ multiple, mutually immiscible liquid drops, characterized by Laplace and Young-Laplace law behavior. This method recognizes that it is impossible to define curvature at a contact point between three mutually immiscible fluids, and so it relies on point thermodynamic arguments [35] which remove the need to measure interface curvature. We note that, in a different context (that drop break-up), this essential problem was first recognized and solved by the same essential idea by Zaleski *et al.*, as long ago as 1995 [36]. We will use the notation of reference [18].

Before defining a behavior (1) between embedding and vesicle fluids and (2) between two different vesicle fluids, we remark that, in the case of many vesicles, Young-Laplace law contact behavior is inappropriate, and ballistic contact between two suspended vesicles may be rare, due to a the presence of a lubrication layer of the fluid in which the vesicles are embedded. We effectively ensure that such a lubricating layer always remains in the contact, in this work.

(1) Vesicle-embedding fluid interaction. Since no Laplace-Young contact need exist for vesicles, it is possible to revert to a body force density based upon the computation of the curvature between the embedding, 0, fluid and the mth fluid, which we denote K^{0m}, $m \neq 0, m < (M-1)$. Consider a drop of fluid $m \neq 0$ to be the interior of a vesicle embedded or supported in the background plasma of fluid $m \equiv 0$. Let us here denote the color degree of freedom on the LBM distribution function by a superscript as follows: f_i^m. The associated vesicle fluid density, ρ_m, phase field relative to the embedding fluid, ρ_{0m}^N and interfacial normals, $\hat{\mathbf{n}}_{0m}$, are defined in Eqs. (61), (63), and (64) of Ref. [18], respectively. The local membrane curvature for the mth vesicle is computed by adapting Eq. (15):

$$K_{m0} = \hat{n}_{m0x}\hat{n}_{m0y}\left(\frac{\partial \hat{n}_{m0y}}{\partial x} + \frac{\partial \hat{n}_{m0x}}{\partial y}\right) - \hat{n}_{m0y}^2\frac{\partial \hat{n}_{m0x}}{\partial x} - \hat{n}_{m0x}^2\frac{\partial \hat{n}_{m0y}}{\partial y}. \tag{28}$$

The appropriate body-force density for the mth vesicle fluid and membrane is simply obtained from Eq. (20) of the previous subsection of this article, with $K \to K_{m0}$. Finally, the postcollision fluid-component segregation step is performed using Eq. (69) of Ref. [18].

(2) Vesicle-vesicle fluid interaction. Vesicles in close approach may trap a film of the fluid in which they are embedded. In principle, this film may be thinner than the width of the membrane in our model (which was quantified in Sec. III D). We chose to impose an interface body force density corresponding to large Laplace law interfacial tension between vesicle fluid $n \neq 0$ and vesicle fluid $m \neq 0$, using precisely the local interface method of Ref. [18], without any modification whatsoever. This choice guarantees that vesicles do not coalesce and provides a well-defined behavior, but it also ensures that a thin layer embedding fluid is induced to remain in the region between two independent vesicles.

We reserve a discussion of the consequences of (2) to the Results and Discussion section.

IV. RESULTS AND DISCUSSION

Throughout this section, we will use LB units. It is possible straightforwardly to calibrate simulations using dimensionless groups. We aim to present results which demonstrate the key credentials of our purely Eulerian, MCLB-based, membrane method and to provide computational validation. Since the purpose of this work is to furnish a new means of simulating flows containing multiple vesicles, we are concerned with membranes which are close to mechanical equilibrium, at all times, and we will not consider the dynamics of membrane relaxation. Recall that the vesicle membrane material is assumed to have a preferred curvature, $K_0 = 0$ (corresponding to a sheet of material which is naturally flat), all simulation data presented were obtained using that LB model usually designated the $D2Q9$, single relaxation time "LBGK" variant [13], and no viscosity contrast was applied between the internal and external fluids.

Unless otherwise stated, $\tau = 1$ for both internal and external fluids and vesicles were all initialized with an ellipsoidal shape, characterized by a semimajor (semiminor) axis length of $a = 22$ ($b = 18$) lattice units. Euler's approximate expression $\pi\sqrt{2(a^2 + b^2)}$ for the perimeter of the ellipse (appropriate for such as aspect ratio as ours, here) was used to compute an initial vesicle "volume" to length ratio close to ten (9.85) lattice units. The area (a conserved quantity, of course) is, accordingly, $A_0 = \pi ab$ for all the data presented. Some data use $\tau \neq 1$ and vary the initial vesicle size, in order to make valid comparisons with other workers' data or to verify the robustness of our model.

Figure 1 shows, for what we anticipate is a typical parametrization, pressure, and microcurrent of a pair of aligned, stationary bicuspid vesicle membranes. The interfacial microcurrent or spurious velocity field which arises in MCLB interfaces is clearly small for the parametrization used here, due in part to the fact that the internal and external fluids are at similar pressure (that inside the vesicle being slightly lower than that in the embedding fluid). The microcurrent estimates the error attending the analysis of the Appendix, since it alone is responsible for any unphysical cross-membrane fluxes. Experience with Laplace law interfaces strongly suggests microcurrent activity may be regulated by using the smallest possible values of parameters α and σ.

The remainder of our results aim to validate and demonstrate, in particular, that multiple vesicles induced to flow past each other retain their individual integrity and behave in a physically correct manner throughout the encounter. Given the scope of extant methods on single vesicles, the latter data are key to potential utility of this work.

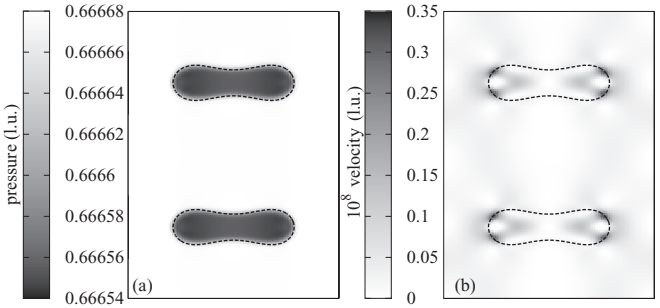

FIG. 1. Note that the microcurrent activity (right panel) is greatly amplified in this figure. The left panel depicts the pressure field. For the final simulation state of two parallel vesicles, shown in this figure, the membrane compressibility, or interface length parameter, $\alpha = 0.015$ lattice units, the interfacial tension parameter $\sigma = 0.008$ lattice units, the bending rigidity $\kappa = 0.55$, and the membrane's preferred length is 176. The final length of both vesicles is 174 lattice units. Both the steady-state pressure step and the interfacial microcurrent activity are very small and localized for this parametrization.

A. Isolated vesicle at rest

A significant excess length is required if a bicuspid shape is to emerge as the final vesicle shape. Thus, the preferred length of the vesicle membrane is set to be a factor $Q_0 = 1.4$ greater than the initial length, i.e., parameter $L_0 = 176$ lattice units, unless stated otherwise. For sufficiently large values of interface compressibility α (see below) this target value of L_0 is, typically, reached within 10^4 time steps, with the final value of the measured length lying within 3.5% of the set value. Length alone is not a good indicator of the mechanical equilibrium, or steady state. While L approaches final L_0 promptly, the equilibrium vesicle shape takes longer to emerge. It should also be noted that the parameter α, should be chosen to maintain membrane incompressibility in dynamic simulations.

We quantify the effect of the model's finite interface width by consider an isolated vesicle subject to shear flow, in the next subsection.

The data presented in Fig. 2 illustrate the influence of the bending rigidity, κ, on dynamics. For Fig. 2, $\alpha = 0.07$, $\sigma = 0.008$, $L_0 = 176$ (corresponding to $Q_0 = 1.4$), and $T = 4.5 \times 10^4$. These values are all consistent with a bicuspid shape when the bending rigidity lies in the range $0.3 \geqslant \kappa \geqslant 0.003$. For a given time, we note that the larger values of κ give larger aspect ratios (the aspect ratio of the $\kappa = 0.3$ data, shown, is approximately $11/3$) and better resemble the shape of erythrocytes. For $\kappa = 0.3$, $\sqrt{\kappa/\sigma} \simeq 6$. Inequality $\sqrt{\kappa/\sigma} < a$ characterizes biological objects. Data produced for $\kappa = 0.55$, $\sigma = 2 \times 10^{-5}$ (not shown), corresponding to $\sqrt{\kappa/\sigma} \simeq 10a$, with a the initial vesicle semimajor axis recall, produce a shape very similar to that shown with $\kappa = 0.3$ but with a still larger aspect ratio ($11/3$).

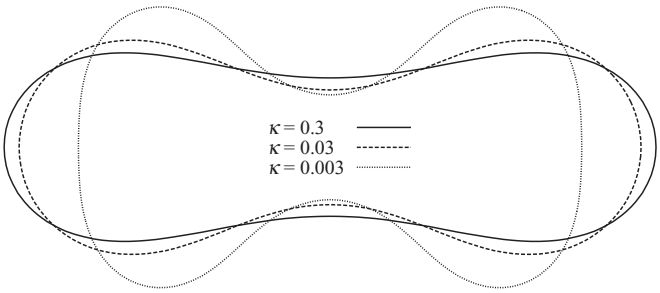

FIG. 2. For the membrane shapes shown in this figure, the interface length parameter $\alpha = 0.07$ lattice units, the interfacial tension parameter $\sigma = 0.008$ lattice units, and the membrane's preferred length is 176 and the time $T = 4.5^4$. The bending rigidity is varied $0.3 \geqslant \kappa \geqslant 0.003$. A bicuspid shape clearly emerges for a wide range of bending rigidities, but more rapidly for larger value of κ.

The data presented in Fig. 3 illustrate the influence of the length relaxation parameter, or membrane compressibility, α. We expect that α will have an important influence on relaxation dynamics of the membrane but neglect this matter, since a majority of the applications we envisage will require the membrane to be close to a mechanical equilibrium at all times, choosing to concentrate instead on the influence of α upon final equilibrium shape. That said, practical considerations press the need for a broad range of usable parameters. Figure 3 was compiled for the following data (all stated in lattice units or dimensionless): $\kappa = 0.5$, $\sigma = 0.008$, $L_0 = 176$ ($Q_0 = 1.4$). The preferred length is achieved, to within 5%, only for $\alpha > 0.15$.

As one might expect, the effect of the membrane compressibility, α, must be considered alongside the chosen value of interfacial tension, σ. To understand the connection, observe that the pressure step across the vesicle membrane is small for all shapes, irrespective of the value of bending rigidity, κ. It is tempting to neglect the role of κ and to consider a form of local Laplace law behavior in the membrane, characterized by an effective interfacial tension $\sigma - \alpha(1 - \frac{L}{L_0})$. On approximating the local pressure step to zero and canceling the local curvature

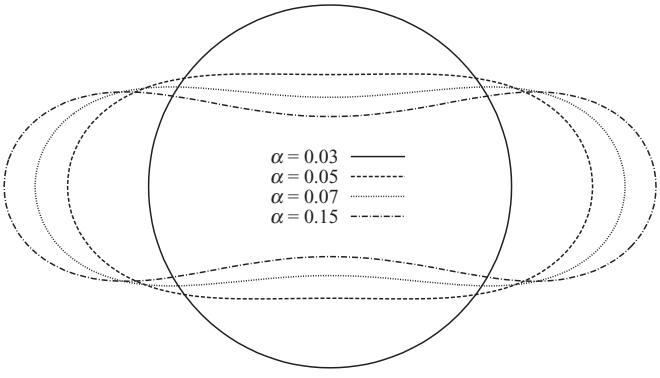

FIG. 3. For the final membrane shapes shown in this figure, the bending rigidity parameter, $\kappa = 0.55$ lattice units, the interfacial tension parameter $\sigma = 0.008$ lattice units, and the preferred length of the membrane $L_0 = 176$. The interface length parameter, $0.03 \leqslant \alpha \leqslant 0.15$ lattice units. A bicuspid shape clearly emerges for value of $\alpha > 0.05$, although the preferred value of length is reached only to within 5% for $\alpha > 0.15$.

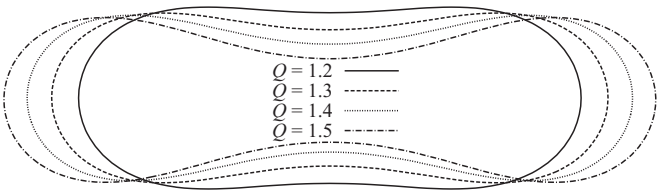

FIG. 4. For the final membrane shapes shown in this figure, the bending rigidity parameter, $\kappa = 0.55$ lattice units, the interfacial tension parameter $\sigma = 0.008$ lattice units, the membrane compressibility, $\alpha = 0.15$ lattice units, and the preferred lengths of the membrane L_0, determined also by the parameter Q_0, were specified as follows: $L_0 = 151$ ($Q_0 = 1.2$), $L_0 = 163$ ($Q_0 = 1.3$), $L_0 = 176$ ($Q_0 = 1.4$), and $L_0 = 188$ ($Q_0 = 1.5$).

(which is not zero, note), we obtain $\sigma - \alpha(1 - \frac{L}{L_0}) = 0$, which may be rearranged to provide a useful expression for the final length of the membrane at mechanical equilibrium:

$$L = \min\left[L_0\left(1 - \frac{\sigma}{\alpha}\right), 2\sqrt{\pi A_0}\right], \tag{29}$$

in which the ration σ/α is dimensionless. The last result recognizes that the length of the membrane cannot be less the perimeter of a circle of area equal to the initial area, A_0. The last equation is useful in calibrating membrane shape. In fact, all tested parametrizations obey Eq. (29), which appears to relate parameters L, σ, κ, α, and L_0 very well.

Clearly, our model's interface compressibility parameter affects the final length of the membrane, at steady state. However, once a final vesicle membrane length is achieved, that length is maintained constant, which is consistent with our assumptions, particularly of a membrane which does not compress.

The data presented in Fig. 4 aim to illustrate the influence of the preferred length, L_0, or Q_0 on the final shape. For this data, the bending rigidity parameter, $\kappa = 0.55$, $\sigma = 0.008$, $\alpha = 0.15$, and the preferred lengths of the membrane L_0, determined also by the parameter Q_0, were specified as follows: $L_0 = 151$ ($Q_0 = 1.2$), $L_0 = 163$ ($Q_0 = 1.3$), $L_0 = 176$ ($Q_0 = 1.4$), and $L_0 = 188$ ($Q_0 = 1.5$).

To validate the static properties of the vesicles which emerge in our method, we employ the dimensionless deflation, reduced volume, or swelling parameter, defined after Kaoui *et al.* [3,4]. Deflation α' (not to be confused with our interface compressibility parameter) is defined in terms of the vesicle perimeter, L, as follows:

$$\alpha' \equiv \frac{S}{\pi\left(\frac{L^2}{2\pi}\right)} = \frac{4\pi S}{L^2}, \tag{30}$$

in which S denotes the measured area of the vesicle. Deflation, in two dimensions, is the ratio of the area of a circle also having perimeter L to the vesicle area, S. Figure 5 shows a range of final vesicle shapes, classified by the computed value of α', obtained using the present method. These static shapes are independent of the value of κ used (in agreement with Kaoui *et al.* [3,4]) and correspond very well with those shown in Fig. 2 of Ref. [5], which were obtained using a boundary-integral based technique. Note that the shapes in Fig. 5 are rotated by $\pi/2$ radians relative to others presented in this section solely to facilitate comparisons with data in

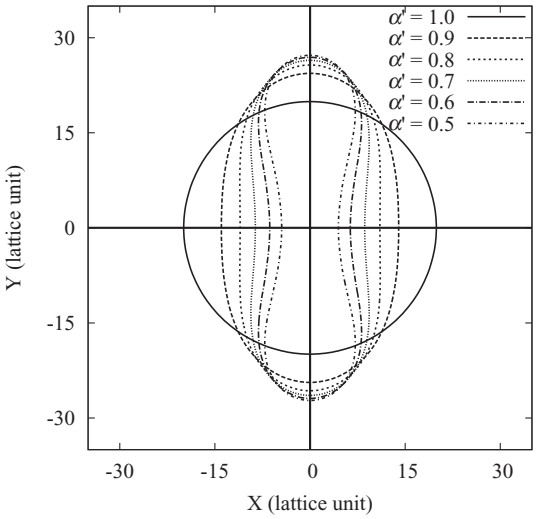

FIG. 5. Static validation. In these data, parameter α' denotes vesicle deflation. The figure shows final vesicle shapes for a range of reduced volume, $\alpha' = 4\pi S\ L^2$, where S denotes the measured area of the vesicle. The final vesicle shapes shown here are in good agreement with those obtained by Kaoui *et al.* [5], who use an unrelated boundary-integral-based technique.

Ref. [5]. The data presented in this figure were obtained using a resolution which corresponds as closely as possible to that used by Kaoui *et al.* In the next section we will use the deflation to perform computational validations.

B. Single vesicle in confined flow

Using a boundary integral method, Kaoui *et al.* [4] computed the migration of a single, deformable bicuspid vesicle in an unbounded Poiseuille flow [4] and Secomb and Pries, and their coworkers, have conducted leading *in silico* studies of single red blood cells, which often include impressive detail of the complex interaction between the cell and the containing vessel wall (a glycocalyx-lined capillary should be treated as a compressible porous medium [37]).

Convergence to the narrow interface limit in our model and its relationship to resolution was assessed by applying a fixed shear to a confined vesicle, characterized by a fixed set of parameters, while increasing system resolution. Figure 6 shows a progression in steady-state vesicle deformation, $(L - B)/(L + B)$, until a certain level of resolution. Note that the inset image shows convergence to steady shape and angle of inclination. R_0 denotes the initially circular vesicle's radius and, temporarily, L (B) denotes the semimajor (semiminor) axis length of the steady-state shape (inset image).

Figure 7 represents a line of equally spaced, identical 2D vesicles, each parameterized like those in previous figures ($\sigma = 0.008$ lattice units, $\kappa = 0.55$ lattice units, $\alpha = 0.15$ lattice units, $Q_0 = 1.4$) to produce a bicuspid shape in mechanical equilibrium. These vesicles are confined between infinite horizontal boundaries $y = 0,122$ lattice units and subject to a horizontal body force density of 2.0×10^{-6} lattice units, which accelerates them in the axial direction. The MCLB distribution functions were constrained to be symmetric about the horizontal symmetry axis in order to minimize simulation effort (a fully resolved simulation at

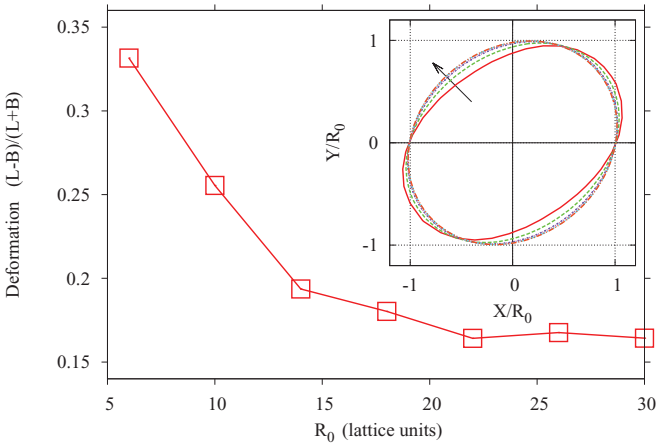

FIG. 6. (Color online) Convergence to the narrow interface limit and its relationship to resolution. A fixed shear was applied to a confined vesicle, characterized by a fixed set of parameters, while increasing system resolution. There is a progression in steady-state vesicle deformation, $(L - B)/(L + B)$, until a certain level of resolution. The inset image confirms that the steady angle of inclination is invariant. R_0 denotes the initial vesicle radius, and, for this figure only, L (B) denotes the semimajor (semiminor) axis length of the steady-state shape (inset image). For this data, $\alpha' = 1.0$, $\chi = 0.4$, Ca $= 1.0$, Re $= 9.45 \times 10^{-2}$ or Kaoui *et al.* [4].

Re > 1 will introduce the possibility of lateral migration of a deformed vesicle which has lost its front-to-back symmetry). The membrane length did not change significantly, as flow was applied, indicating an incompressible membrane. The data of the figure show the resulting steady state of the system. The data in Fig. 7 clearly show the vesicle membrane behaving as a fluid. Consider the stagnation point at the intersection of the horizontal symmetry axis and vesicle membrane, to the right of the figure. Above (below) this point, the internal and external fluids in immediate contact with the membrane have a positive (negative) y-velocity component. In the continuum approximation the relative motion of the separated fluids must vanish at a boundary, and so, relative to the boundary, there can be no normal component of velocity and the fluids layer confined to the interface, or membrane, is conserved. This is consistent with our assumptions. In fact, the same observations apply to a simple droplet, which does not have a conserved surface area.

In the data of Fig. 8 the vesicle assumes a more familiar shape, in response to a different set of simulation parameters (see figure caption). It should be noted that symmetry was enforced along the midchannel, in the data of Figs. 7 and 8. Therefore, the vesicle shape depicted here may not represent the stable state of an unconstrained system [3].

In order to validate the present model computationally, we choose to compare data from our model with Kaoui's data for a single vesicle in confined, shear flow [5]. For a range of Kaoui's confinement parameter χ, we plot, in Fig. 9, the inclination of the steady-state vesicle, quantified by the angle subtended at the shear direction of the vesicle long axis, as a function of the vesicle deflation parameter, α'. The data of Kaoui *et al.* was obtained manually from the Fig. 3, presented in Ref. [5]. The LBGK relaxation parameter $\tau = 1.2$ for these data, the simulation lattice measured 60×120 lattice units,

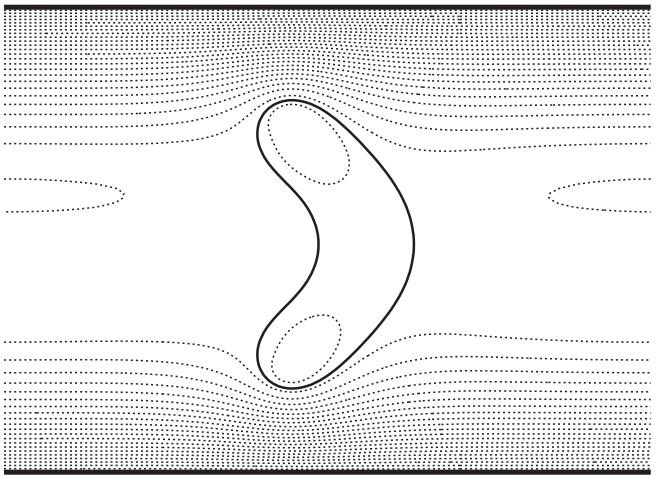

FIG. 7. For the final membrane shape (solid line) and steady-state flow (broken lines, see below) shown here, $\sigma = 0.008$ lattice units, $\kappa = 0.55$ lattice units, $\alpha = 0.15$ lattice units, $Q_0 = 1.4$. The vesicle depicted is one of an infinite sequence of identical, equally spaced vesicles which are sedimenting under gravity. The gravitational body force density applied to the vesicle fluid (only) was 2.0×10^{-6} lattice units. The broken lines image relative flow: They represent contours of constant value of the rectangular stream function, computed in the rest frame of the vesicles. The lack of symmetry is solely an artifact of the plotting package. It should be noted that symmetry was enforced along the midchannel. Therefore, the vesicle shape depicted here may not represent the stable state of an unconstrained system.

the initial vesicle radius being 12, to match the resolution used by Kaoui *et al*. The data presented are insensitive to doubling the simulation resolution. These facts encourage a view that our method is sensibly robust and practical. Given that the two techniques are very different, the agreement between data

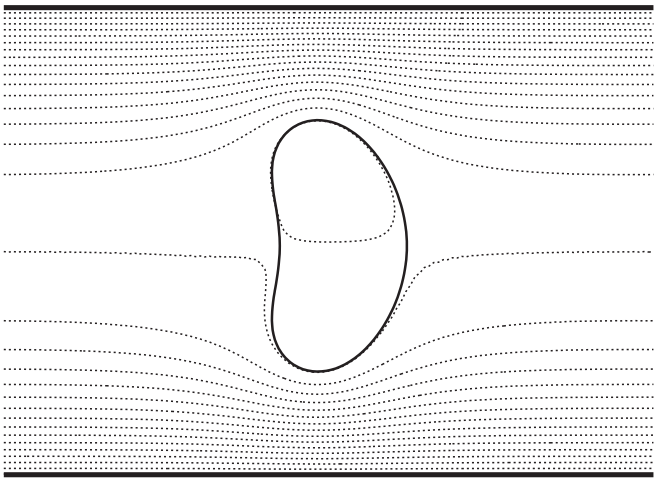

FIG. 8. For the more familiar final membrane shape (solid line) and steady-state flow (broken lines, see below) shown here, $\sigma = 0.016$ lattice units, $\kappa = 0.35$ lattice units, $\alpha = 0.15$ lattice units, $Q_0 = 1.4$. The vesicle depicted is one of an infinite sequence of identical, equally spaced vesicles which are sedimenting under gravity. The gravitational body force density applied to the vesicle fluid (only) was increased to 1.0×10^{-5} lattice units. Again, any lack of symmetry is an artifact of the plotting package.

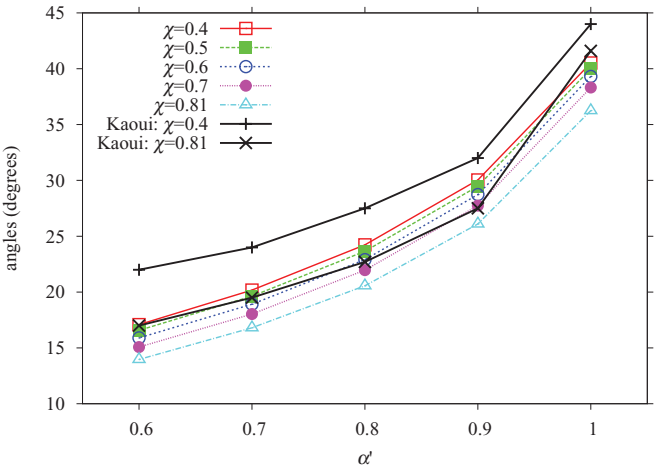

FIG. 9. (Color online) In this data, parameter α' denotes vesicle deflation, not interface compressibility. Validation of the present model against Kaoui's data for a single vesicle in confined, shear flow [5], for a range of confinement parameter χ. The inclination of the steady-state vesicle, quantified by the angle subtended at the shear direction of the vesicle long axis is plotted as a function of deflation, α. The LBGK relaxation parameter $\tau = 1.2$ for these data, the simulation lattice measured 60×120 lattice units, the initial vesicle radius being 12, to match the resolution used by Kaoui *et al*.

from the present model and that obtained by Kaoui *et al*. is good, with our data spanning a similar range of observations to that of Kaoui *et al*., while exhibiting a similar trend.

C. Multiple sedimenting vesicles in unbounded flow

The data presented in this section aim to demonstrate our model's facility with multiple vesicles, which encounter each other in flow. We consider an infinite 2D array of identical bi-cuspid vesicles, each represented by a different fluid. The image in Fig. 10 is the unit cell. The embedding fluid, and the fluid which fills both vesicles are all mutually immiscible but have identical physical properties. The interface between the vesicle fluids is characterized by a Laplace law interfacial tension [18].

Consider the array of static vesicles depicted in part (a) of Fig. 10. To these vesicles, body forces will be applied. Suppose the initial vertical spacing between horizontal layers is reduced to zero, that is, vesicles are initialized to overlap. If the interfacial tension between mutually immiscible vesicle fluids, σ', is set to be large compared with membrane interfacial tension (here $\sigma' = 10\sigma$), then even vesicles initialized in direct contact (without a film of embedding fluid) will separate, embedding fluid flowing into the narrow gap. The interface in MCLB simulation is not discontinuous. In our variant, the interfacial phase field varies as $\tanh(\beta n)$. Recall that n denotes distance measured in the direction of the interfacial normal (see the Appendix). At mechanical equilibrium, define the width, W, of the layer of embedding fluid in the contact, after equilibration:

$$W = \frac{\int \rho_0(n) n^2 \, dn}{\int \rho_0(n) \, dn}. \tag{31}$$

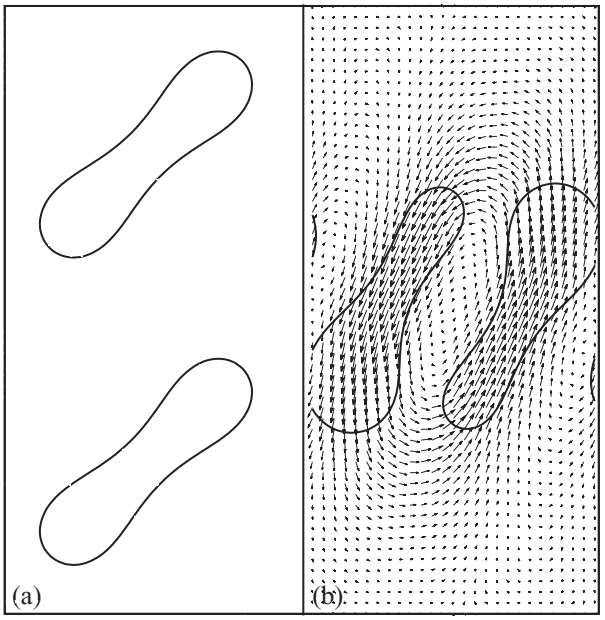

FIG. 10. (a) The solid line represents the initial shape of a multiple vesicle simulation, showing the two vesicles which make up the unit cell of this simulation, which uses periodic boundary conditions on all sides of the box, or unit cell. The static bicuspid vesicles and embedding fluid are comprised of mutually immiscible fluids. The vesicle membrane parameters are $\sigma = 0.008$ lattice units, $\kappa = 0.55$ lattice units, $\alpha = 0.15$ lattice units, and $Q_0 = 1.4$. (b) Evolved state of the multiple vesicle simulation depicted in (a) after a body-force density of 5.0×10^{-5} lattice units has been applied for 1.25×10^4 time steps. In (b) the relative velocity field is coarse grained, having been plotted every third lattice site, for clarity.

Replacing the integrations with appropriate summations (see Sec. III D), we measure $W = 2.37$ from simulations, which is small. Indeed, flow-induced ballistic contact between vesicles was observed not to arise in simulations. Hence, it is possible to set σ' small in practice. This freedom to select a small vesicle-vesicle fluid interfacial tension results in a small external force density in the region where membranes encounter each other. Consequently, one will observe only hydrodynamics (but see below) in that region, which may therefore be characterized as a parallel, locally flat membranes confining a layer of embedding fluid. No vesicle contact lubrication force is postulated in this data presented here. In Sec. III D, we have calculated a characteristic interface width in our model which is greater than the lattice spacing, recall, and it may be argued that a thinner layer of embedding fluid is improperly resolved and that an effective lubrication force should therefore be necessary above the sublattice threshold. Such a lubrication correction was proposed for LB by Nguyen and Ladd [38]. The approach of Nguyen and Ladd might be applied to our model, though to overcome the destabilizing effect previously noted, attending the imposition of another force, larger resolution would be required. We return to this matter in our conclusions.

For the data of Fig. 10, the static vesicle membrane parameters are $\sigma = 0.008$ lattice units, $\kappa = 0.55$ lattice units, $\alpha = 0.15$ lattice units, and $Q_0 = 1.4$. From the initial steady state in part (a) of Fig. 10, the upper (lower) vesicle is induced by a body-force density, of magnitude 5.0×10^{-5} lattice units, to move downwards (upwards). The magnitude of the acceleration of both vesicles is identical. Their horizontal spacing means that, in "counter-sedimenting" they must pass close to each other at 1.25×10^4 time steps, while undergoing noticeable deformation. The image in part (b) of Fig. 10 represents the later state of the flow field and the membrane boundaries. Note that the velocity field is represented by coarse-grained vector field (see caption), since it is not possible to define a stream function for an unbounded environment. We note, also, that interfacial tension postulated to act in the interface between vesicle fluids is very small and has no observable effect on flow.

V. CONCLUSION AND FURTHER WORK

We have presented an extension to a 2D multiple immiscible fluid component lattice Boltzmann simulation method. While preserving the underlying simplicity of the algorithm and all its computational advantages, the resulting fluid-vesicle method extends the physics of a fluid-fluid "Laplace-law" interface, to impart additional membrane properties of preferred curvature, bending rigidity and membrane compressibility, producing a simulated vesicle with conserved membrane length and volume, embedded in a viscous fluid. Crucially, the method is shown to generalize straightforwardly to multiple vesicles in flow. Uniquely, our method is completely Eulerian and uses only the framework of multicomponent lattice Boltzmann equation, and we make no use whatsoever of, e.g., remeshing or hybrid Lagrangian schemes. None of our easy-to-implement algorithmic extensions further compromise the multiple-component lattice Boltzmann equation method's inherent affinity with parallel computation, the model has an extensive stable parameter space, and the value of lattice Boltzmann method collision parameter, τ, is not restricted by their use.

The extended, multiple immiscible component lattice Boltzmann method for vesicles we present is an evolution of a scheme for multiple liquids [18,20]. It benefits from its demonstrably correct interfacial kinematics and near-complete absence of unphysical fluxes and spurious velocities. The vesicles in the present model can access the biological regime and the method retains the advantageous scaling of computational effort, as the number of vesicles is increased, reported in related previous work [17]. It should be noted that the most widely used multiple component lattice Boltzmann technique, due originally to Shan and Chen [21] has recently been extended, effectively to the regime of interrupted coalescence utilized here. So-called double-belt Shan-Chen implementations [39] therefore provide, we believe, a potential alternative vehicle for our method. Whatever its encapsulation, a model such as that we have advanced, with deformable vesicles, requires a resolution which, currently, confines its application to capillary scales. We propose below certain remedies of restricted yet worthwhile scope. However, we note that, to address cardiovascular scales, the lattice Boltzmann method-based approach of Melchionna *et al.* [10,11], which employs rigid, minimal particulates, is currently the only practical approach (and one algorithmically consistent with the current model).

We have noted the interface in the present model is of finite width, which, while small (Sec. III D), introduces an

unphysical length scale, the presence of which will be felt most as simulation resolution decreases. In the future, by adjusting the membrane force density distribution weight function, we aim to sharpen the membrane force density and, hence, reduce the effective width. Once this question is answered, an appropriate lubrication force can be consistently introduced. A 3D model is also required. The appropriate, purely normal force per unit *area* of interface is given in the Appendix, the appropriate weight function being that used here, namely, $\nabla\rho^N$. It would be necessary only to devise a robust membrane area measure.

The present work paves a way to an equivalent 3D method (see the Appendix) and, hence, to accurate and feasible deformable particle-laden flow applications in the biosciences. To address larger scales, this objective will necessitate simplification, multiscaling and appeal to ideas embedded in such models as that due to Melchionna *et al*. [10,11].

APPENDIX: DERIVATION OF MEMBRANE FORCES

Here we present detail in the derivation of the expressions, given in Sec. III, for the force contributions acting on a 2D membrane length element, ds. Three expressions are obtained by taking the variational derivatives of the appropriate free energy contribution $A_L[\mathbf{r}]$, $A_S[\mathbf{r}]$ and $A_K[\mathbf{r}]$, respectively. These energies are defined in Sec. III.

Recall that the parameter, $t \in [0, L_0]$, corresponds to length measured along the undeformed membrane at mechanical equilibrium and that $u(\dot{x},\dot{y}) \equiv \sqrt{\dot{x}^2+\dot{y}^2}$ has no explicit t dependence. We denote the unit vector normal to the membrane $\hat{\mathbf{n}}(t)$ with $\hat{\mathbf{n}} = (\dot{y}/u(\dot{x},\dot{y}), -\dot{x}/u(\dot{x},\dot{y}))$. For brevity, in the remainder of this subsection we shall simply write u.

Let us consider the excess free energy associated with a length perturbation. The variational derivative of $A_L[\mathbf{r}]$ with respect to x gives the x component of the membrane force contribution, $\mathbf{F}_L$:

$$\mathbf{F}_{Lx} = -\frac{\delta}{\delta x}\left[\frac{\alpha}{2}\int_0^{L_0}(u-1)^2 dt\right]. \tag{A1}$$

Now, defining the variational derivative in the usual way, using the Euler-Lagrange equations [19] and substituting for $u = \sqrt{\dot{x}^2+\dot{y}^2}$, we have

$$\mathbf{F}_{Lx} = -\frac{\alpha}{2}\left[\frac{\partial}{\partial x} - \frac{d}{dt}\left(\frac{\partial}{\partial \dot{x}}\right)\right](\sqrt{\dot{x}^2+\dot{y}^2}-1)^2, \tag{A2}$$

and, upon noting that there is no explicit dependence on x and t in the expression $(\sqrt{\dot{x}^2+\dot{y}^2}-1)^2$, straightforward algebra yields

$$\mathbf{F}_{Lx} = \alpha\ddot{x} + \alpha\dot{y}\left[\frac{\dot{x}\ddot{y}-\dot{y}\ddot{x}}{(\dot{x}^2+\dot{y}^2)^{3/2}}\right] \tag{A3}$$

in which equation the term in square brackets corresponds to the curvature, K. The y component of this force is obtained from the variational derivative on $y(t)$, yielding

$$\mathbf{F}_L = \alpha(\ddot{x},\ddot{y}) + \alpha K(\dot{y},-\dot{x}) = \alpha\frac{d^2\mathbf{r}}{dt^2} + \alpha K(\dot{y},-\dot{x}). \tag{A4}$$

This general expression for $\mathbf{F}_L$ may now be adapted into a particularly advantageous form, for MCLB computation, by assuming rapid relaxation of membrane stresses on flow timescales and, consistent with this, that the strain is uniform throughout the membrane. Recalling the role of parameter, t, we write $\frac{ds}{dt} = \frac{L}{L_0}$. Now, $(\dot{x},\dot{y}) = \frac{d\mathbf{r}}{dt} = \frac{ds}{dt}\frac{d\mathbf{r}}{ds}$. Using the definition of the unit tangent, $\hat{\mathbf{t}}$, and our assumptions we have $(\dot{x},\dot{y}) = \frac{L}{L_0}\hat{\mathbf{t}}$ and, hence,

$$(\dot{y},-\dot{x}) = \frac{L}{L_0}\hat{\mathbf{n}}. \tag{A5}$$

Next write $\frac{d^2\mathbf{r}}{dt^2} = \frac{d}{dt}(\frac{d\mathbf{r}}{ds}\frac{ds}{dt}) = \frac{d}{dt}(\hat{\mathbf{t}}\frac{ds}{dt}) = \hat{t}\frac{d^2s}{dt^2} + \frac{ds}{dt}\frac{d}{dt}\hat{\mathbf{t}} = \hat{\mathbf{t}}\frac{d^2s}{dt^2} + (\frac{ds}{dt})^2\frac{d}{ds}\hat{\mathbf{t}}$. Given $\frac{ds}{dt}$ is constant throughout the membrane, $\frac{d^2s}{dt^2} = 0$ and, being careful to take the normal in the direction pointing away from the region enclosed by the curve, we obtain

$$\frac{d^2\mathbf{r}}{dt^2} = \frac{d^2s}{dt^2}\hat{\mathbf{t}} + \left(\frac{ds}{dt}\right)^2 K\hat{\mathbf{n}} = K\left(\frac{L}{L_0}\right)^2\hat{\mathbf{n}}, \tag{A6}$$

where we have used the Frenet-Serret formulas to introduce the local curvature, $K(t)$. On appeal to Eqs. (A5) and (A6), we find an appropriate interface length-conserving force:

$$\mathbf{F}_L = \alpha\frac{L}{L_0}K\left(1-\frac{L}{L_0}\right)\hat{\mathbf{n}}. \tag{A7}$$

The derivation of the interfacial tension force, $\mathbf{F}_S$, is similar to that for $\mathbf{F}_L$. By direct use of the Euler-Lagrange equations [19] and the definition of curvature in two dimensions we obtain

$$\mathbf{F}_S = -\frac{\delta}{\delta\mathbf{r}}\left(\sigma\int_0^{L_0} u\,dt\right) = \sigma K(\dot{y},-\dot{x}), \tag{A8}$$

in general and, invoking our assumption of rapid relaxation of membrane stresses, in the form of Eq. (A5), it follows:

$$\mathbf{F}_S = -\sigma\frac{L}{L_0}K\hat{\mathbf{n}}. \tag{A9}$$

The derivation of the curvature contribution, $\mathbf{F}_K$, is slightly more involved. The variational derivative in the right hand side of Eq. (5) may clearly be written as the sum of three contributions:

$$\mathbf{F}_K = -\frac{\kappa}{2}\frac{\delta}{\delta\mathbf{r}}\left(\int_0^{L_0} K^2 u dt + K_0^2\int_0^{L_0} u\,dt - 2K_0\int_0^{L_0} Ku\,dt\right). \tag{A10}$$

The second term in the right-hand side of the above equation is very similar to the expression for $\mathbf{F}_S$ and clearly

$$-\frac{\delta}{\delta\mathbf{r}}\left(K_0^2\int_0^{L_0} u\,dt\right) = K_0^2\frac{L}{L_0}K\hat{\mathbf{n}}. \tag{A11}$$

The third term in expression (A10) gives zero, following the method we now apply to the first term. In Eq. (A10), the first term has an integrand which depends upon the second derivatives, $\ddot{x}$ and $\ddot{y}$ (through K). Accordingly, it is necessary to use extended Euler-Lagrange equations [19] for its variational

derivative. On noting that K^2u has no explicit x dependence:

$$\frac{\delta}{\delta x}\left(\int_0^{L_0} K^2u\,dt\right) = -\frac{d}{dt}\left[\frac{\partial}{\partial \dot{x}} - \frac{d}{dt}\left(\frac{\partial}{\partial \ddot{x}}\right)\right]K^2u. \tag{A12}$$

Now, it is straightforward to show $\frac{\partial}{\partial \dot{x}}K^2u = -\frac{2K\dot{y}}{u^2}$ and $\frac{\partial}{\partial \ddot{x}}K^2u = \frac{K^2\dot{x}}{u} - \frac{4K\dot{x}^2\ddot{y}-2K\dot{y}^2\ddot{y}-6K\dot{x}\dot{y}\ddot{x}}{u^4}$. From these results, it is possible to obtain the following, after some algebra:

$$\left[\frac{\partial}{\partial \dot{x}} - \frac{d}{dt}\left(\frac{\partial}{\partial \ddot{x}}\right)\right]K^2u = -\frac{K^2\dot{x}}{u} + \frac{2\dot{y}}{u^2}\frac{dK}{dt}. \tag{A13}$$

Substituting Eq. (A13) into the Eq. (A12), performing the time differentiation, and using the identity $u\frac{du}{dt} = \dot{x}\ddot{x} + \dot{y}\ddot{y}$ there results

$$\frac{\delta}{\delta x}\left(\int_0^{L_0} K^2u\,dt\right) = K^3\dot{y} - \frac{2\dot{y}}{u^2}\left(\frac{d^2K}{dt^2} - \frac{1}{u}\frac{du}{dt}\frac{dK}{dt}\right). \tag{A14}$$

Now, using the Chain Rule, one can show $\frac{d^2K}{ds^2} = \frac{1}{u^2}\frac{d^2K}{dt^2} - \frac{1}{u^3}\frac{dK}{dt}\frac{dK}{dt}$ and hence we find, for the first term in expression (A10):

$$\frac{\delta}{\delta x}\left(\int_0^{L_0} K^2u\,dt\right) = K^3\dot{y} - \frac{2\dot{y}}{u^2}\frac{d^2K}{ds^2}. \tag{A15}$$

The corresponding variational derivative with respect to y is computed in identical fashion. Then, using Eqs. (A5) and (A15), we obtain, for curvature force:

$$\mathbf{F}_K = \kappa\frac{L}{L_0}\left[\frac{1}{2}K\left(K^2 - K_0^2\right) + \frac{d^2K}{ds^2}\right]\hat{\mathbf{n}}. \tag{A16}$$

1. Membrane force in three dimensions

For completeness, we state, here, the normal force on a 3D membrane surface element. Let the surface have instantaneous (preferred) area A (A_0), a single preferred curvature, H_0, a mean local curvature $H = (K_1 + K_2)/2$ and a Gaussian curvature $K = K_1K_2$, where K_1 and K_2 and the principal curvatures. We allow for spatial variation in the bending rigidity, κ. The normal force acing upon, or due to such a membrane is

$$F_n = -2\sigma H + \kappa C + \nabla_s\kappa.\nabla_s(H - H_0) - 2\alpha(A - A_0)H, \tag{A17}$$

where ∇_s is the surface gradient, Δ_s is the Laplace-Beltrami operator, and

$$C = H\left(H^2 - H_0^2\right) + \tfrac{1}{2}\Delta_s H - (H - H_0)K. \tag{A18}$$

2. Interfacial isotropy and Galilean invariance

Here we consider, in detail, the salient isotropy properties of a 2D interface. Explicit reference to the MCLB lattice structure is necessary and we therefore work on a $D2Q9$ lattice, for simplicity and to maintain parity with previous, related work [18].

We consider only that class of LBM interface arising from use of one particular LBM fluid component segregation rule [18,28] and further restrict our attention to the case of a flat interface with any orientation relative to simulation lattice.

We consider (1) a stationary phase field boundary and (2) one embedded in a uniform flow, seeking to demonstrate its isotropic structure and the model's Galilean invariance. Our overall approach is to extract the macroscale motion of the phase field boundary from the expansion of discrete, microscopic dynamics of LBM.

We consider two immiscible fluids, designated red and blue, described by two distribution function components, R_i and B_i. Throughout, we will use the notation of Refs. [28] and [18].

a. Isotropy of the interface

In a uniform fluid at rest, the red fluid density, now denoted for clarity $R \equiv \rho_R = \Sigma_i R_i$, associated with a flat interface, without interfacial tension, and with orientation defined by normal vector $\hat{\mathbf{n}}$, evolves according to the rule

$$R(\mathbf{r}, t + \delta_t) = \sum_{i=0}^{9} R_i(\mathbf{r} - \mathbf{c}_i\delta_t, t), \tag{A19}$$

where, for d'Ortona's segregation [33],

$$R_i(\mathbf{r},t) = \frac{R(\mathbf{r},t)}{\rho(\mathbf{r},t)}f_i + \beta t_i\frac{R(\mathbf{r},t)B(\mathbf{r},t)}{\rho(\mathbf{r},t)}\mathbf{c}_i\cdot\hat{\mathbf{n}}. \tag{A20}$$

In the summation in Eq. (A19), terms with an even (odd) value of i have link weight $t_p = 1/9$ (1/36). The rest link has $t_0 = 4/9$ [32]. The position vector $\mathbf{r}$ is expressed in a coordinate system (x, y) which is aligned with the underlying simulation lattice. In the case of rest fluids, at steady state (moving fluids are treated in the next subsection), we can therefore write

$$R(\mathbf{r}) = \sum_{i=0}^{N} t_i R(\mathbf{r} - \mathbf{c}_i\delta_t) + \frac{\beta}{\rho_0}\hat{\mathbf{n}}\sum_{i=0}^{N} t_i\mathbf{c}_i R(\mathbf{r} - \mathbf{c}_i\delta_t) \times [\rho_0 - R(\mathbf{r} - \mathbf{c}_i\delta_t)], \tag{A21}$$

where all symbols have their usual meaning. In Eq. (A21) we have used the fact that $\rho(\mathbf{r},t) = \rho_0$, $f_i = t_i\rho_0$ for a uniform fluid. By Taylor expanding the terms in the right-hand side, about $\mathbf{r}$, to second-order in the lattice spacing, h, there results, after some algebra:

$$\nabla^2 R - 2\frac{\beta}{h}(\hat{\mathbf{n}}\cdot\nabla)R + 2\frac{\beta}{h\rho_0}(\hat{\mathbf{n}}\cdot\nabla)R^2 = 0. \tag{A22}$$

In the steady-state equation (A22), the usual properties of lattice tensors have been used:

$$\sum_i t_p c_{i\alpha}c_{i\beta} = c_s^2\delta_{\alpha\beta}, \tag{A23}$$

$$\sum_i t_p c_{i\alpha}c_{i\beta}c_{i\gamma}c_{i\delta} = c_s^4(\delta_{\alpha\beta}\delta_{\gamma\delta} + \delta_{\alpha\gamma}\delta_{\beta\delta} + \delta_{\alpha\delta}\delta_{\beta\gamma}), \tag{A24}$$

$$c_s^2 = \frac{1}{3}\frac{h^2}{\delta_t^2}, \tag{A25}$$

where h is the mesh-spacing, i.e., the length of the lattice link characterized by an even value of i. Note that the last result is specific to the $D2Q9$ lattice.

Now, the following rotation of coordinates through angle $\theta = \cos^{-1}(\hat{n}_y/\hat{n}_x)$, measured anticlockwise, into a Cartesian

system aligned with its $\bar{x}$ axis parallel to $\hat{\mathbf{n}}$:

$$\bar{x} = \cos(\theta)x + \sin(\theta)y, \quad \bar{y} = -\sin(\theta)x + \cos(\theta)y \tag{A26}$$

is used to transform Eq. (A22) as follows:

$$\frac{d^2}{d\bar{x}^2}R - 2\frac{\beta}{h}\frac{d}{d\bar{x}}R + 2\frac{\beta}{h\rho_0}\frac{d}{d\bar{x}}R^2 = 0. \tag{A27}$$

Clearly, a first integral of the above equation exists. On supposing that, at large distances in the direction $-\hat{\mathbf{n}}$, R approaches ρ_0 and that at large distances in the direction $+\hat{\mathbf{n}}$, R approaches zero, the solution to this equation is easily shown to be

$$R(\overline{x},\overline{y}) = \rho_0\left[\frac{1-\tanh\left(\frac{\beta}{h}\bar{x}\right)}{2}\right]. \tag{A28}$$

Equation (A28) describes an interface structure and thickness which is independent of interface orientation on the lattice. It agrees with that result which one of us (I.H.) clearly *should* have stated in the Appendix of a previous, more restricted analysis [28].

b. Galilean invariance of the interface motion

It is appropriate to emphasize that, in this subsection, we seek to determine the motion of an interface in a fluid which is supposed to be moving uniformly, for *any* combination of interface orientation and direction of fluid motion, $\mathbf{u}$.

In the case of a fluid in uniform motion, $\mathbf{u}$, containing a flat interface, Eq. (A21) must be generalized to the following:

$$\begin{aligned} &R(\mathbf{r},t+\delta_t) \\ &\quad = \sum_{i=0}^{N}\frac{R(\mathbf{r}-\mathbf{c}_i\delta_t,t)}{\rho_0}f_i^{(0)}(\rho_0,\mathbf{u}) \\ &\qquad + \frac{\beta}{\rho_0}\hat{\mathbf{n}}\sum_{i=0}^{N}t_i\mathbf{c}_i R(\mathbf{r}-\mathbf{c}_i\delta_t,t)(\rho_0 - R(\mathbf{r}-\mathbf{c}_i)\delta_t,t). \end{aligned} \tag{A29}$$

Into Eq. (A29) substitute the usual expression for the $D2Q9$ lattice equilibrium $f_i^{(0)}(\rho_0,\mathbf{u})$ [32]:

$$f_i^{(0)}(\rho_0,\mathbf{u}) = \rho_0 t_p\left(1 + \frac{\mathbf{c}_i\cdot\mathbf{u}}{c_s^2} + \frac{(\mathbf{c}_i\cdot\mathbf{u})^2}{2c_s^4} - \frac{u^2}{2c_s^2}\right) \tag{A30}$$

and take a Taylor expansion about $\mathbf{r}$ and t on both sides. Retaining terms of order δ_t^2, the following equation is obtained straightforwardly but after lengthy calculation:

$$\begin{aligned} \delta_t\frac{\partial R}{\partial t} + \frac{\delta_t^2}{2}\frac{\partial^2 R}{\partial t^2} &= \frac{h^2}{6}\nabla^2 R - \delta_t(\mathbf{u}\cdot\nabla)R + \frac{\delta_t^2}{2}(\mathbf{u}\cdot\nabla)^2 R \\ &\quad - \frac{\beta h}{3}(\hat{\mathbf{n}}\cdot\nabla)R + \frac{\beta h}{3\rho_0}(\hat{\mathbf{n}}\cdot\nabla)R^2. \end{aligned} \tag{A31}$$

In Eq. (A31) all derivatives are taken at position $\mathbf{r}$, time t. Note also that, to obtain Eq. (A31), the isotropy properties of the second and fourth-order $D2Q9$ lattice tensors, reproduced above, have been used in conjunction with the relationship $\delta_t|\mathbf{c}_{ix}| = h$ with i an even number.

Again, the transformation defined in Eq. (A26) is useful. The $\bar{x}$ axis lies parallel to $\hat{\mathbf{n}}$. Expressed in this frame of reference, Eq. (A31) becomes

$$\begin{aligned} &\delta_t\left[\frac{\partial R}{\partial t} + (\overline{\mathbf{u}}\cdot\overline{\nabla})R\right] + \frac{\delta_t^2}{2}\left[\frac{\partial^2 R}{\partial t^2} - (\overline{\mathbf{u}}\cdot\overline{\nabla})^2 R\right] \\ &\quad = \frac{h^2}{6}\overline{\nabla}^2 R - \frac{\beta h}{3}\frac{\partial}{\partial\overline{x}}R + \frac{\beta h}{3\rho_0}\frac{\partial}{\partial\overline{x}}R^2, \end{aligned} \tag{A32}$$

where $\overline{\mathbf{u}}$ denotes the velocity of the fluid, measured in the local, rotated coordinate system $(\overline{x},\overline{y})$. Note that the system $(\overline{x},\overline{y})$ is not dimensionless.

Now, in an infinite, uniform system, there can be no variation of R in the direction parallel to the interface (the $\overline{y}$ direction), whatever the tangential component of velocity, $\overline{u_{\overline{y}}}$. We return to the issue shortly.

Removing $\overline{y}$ derivatives from Eq. (A32) and applying a second transformation to the remaining terms in $\overline{x}$ as follows:

$$\eta = \bar{x} + \overline{u}_{\overline{x}}t, \quad \zeta = \bar{x} - \overline{u}_{\overline{x}}t, \quad t = t, \tag{A33}$$

Eq. (A32) takes the form

$$\begin{aligned} &2\overline{u}_{\overline{x}}\delta_t\frac{\partial R}{\partial\eta} - 2\overline{u}_{\overline{x}}^2\delta_t^2\frac{\partial^2 R}{\partial\eta\partial\zeta} \\ &\quad = \frac{h^2}{6}\left(\frac{\partial^2}{\partial\overline{x}^2}R - 2\frac{\beta}{h}\frac{\partial}{\partial\overline{x}}R + 2\frac{\beta}{h\rho_0}\frac{\partial}{\partial\overline{x}}R^2\right), \end{aligned} \tag{A34}$$

where we note that transformation (A35) has been applied only to terms on the left-hand side. The right-hand sides of Eqs. (A34) and (A27) are structurally identical. By inspection, the solution to this partial differential equation is

$$R(\overline{x},\overline{y},t) = \rho_0\frac{\left[1-\tanh\left(\frac{\beta}{h}\zeta\right)\right]}{2}, \quad \zeta = \bar{x} - \overline{u}_{\overline{x}}t. \tag{A35}$$

Let us return to the case of motion parallel to the interface. Suppose that $\overline{u_{\overline{x}}} = 0$, $\overline{u_{\overline{y}}} \neq 0$. Equation (A32) becomes

$$\begin{aligned} &\delta_t\left(\frac{\partial R}{\partial t} + \overline{u}_{\overline{y}}\frac{\partial R}{\partial\overline{y}}\right) + \frac{\delta_t^2}{2}\left(\frac{\partial^2 R}{\partial t^2} - \overline{u}_{\overline{y}}^2\frac{\partial^2 R}{\partial\overline{y}^2}\right) \\ &\quad = \frac{h^2}{6}\overline{\nabla}^2 R - \frac{\beta h}{3}\frac{\partial}{\partial\overline{x}}R + \frac{\beta h}{3\rho_0}\frac{\partial}{\partial\overline{x}}R^2. \end{aligned} \tag{A36}$$

This equation, the left-hand side of which essentially consists of superposed first- and second-order wave equations, has a separable solution obtained from d'Alembert's solution of the wave equation:

$$R(\overline{x},\overline{y},t) = \rho_0\left\{\frac{\left[1-\tanh\left(\frac{\beta}{h}(\overline{x}-\overline{u}_{\overline{x}t})\right]}{2}\right\}f(\overline{y}-\overline{u}_{\overline{y}}t), \tag{A37}$$

in which the undetermined function, f, must be consistent with the appropriate initial conditions. If the interface is uniform, we obtain $f = \text{const}$. This finding is, of course, perfectly consistent with fluid motion in the direction tangent to the interface, which is implicit throughout the analysis of this section.

Together, Eqs. (A35) and (A37) show that the time development of a flat interface, of the type used in this work, corresponds to advection at the same speed as the underlying fluid, in the direction perpendicular to interface. This is consistent with the kinematic condition

of mutual impenetrability and demonstrates the Galilean invariance of an algorithmic component crucial to this work.

Finally, we note that, subject to approximations made in this section, there are, in our model, no unphysical fluxes across phase field boundary and hence the vesicle membrane.

[1] J. M. Skotheim and T. W. Secomb, Phys. Rev. Lett. **98**, 078301 (2007).
[2] T. W. Secomb, R. Hsu, and A. R. Pries, Microcirculation **9**, 189 (2002).
[3] B. Kaoui, G. Biros, and C. Misbah, Phys. Rev. Lett. **103**, 188101 (2009).
[4] B. Kaoui, G. H. Ristow, I. Cantat, C. Misbah, and W. Zimmermann, Phys. Rev. E **17**, 021903 (2008), and references therein.
[5] B. Kaoui, J. Harting, and C. Misbah, Phys. Rev. E **83**, 066319 (2011).
[6] C. S. Peskin, J. Comput. Phys. **25**, 220 (1977).
[7] J. Zhang, P. C. Johnson, and A. S. Popel, Phys. Biol. **4**, 285 (2007).
[8] T. Krüger, F. Varnik, and D. Raabe, Comp. Math. Appl. **61**, 3485 (2011).
[9] M. M. Dupin, I. Halliday, C. M. Care, L. Alboul, and L. L. Munn, Phys. Rev. E **75**, 066707 (2007).
[10] S. Melchionna, M. Bernaschi, S. Succi, E. Kaxiras, F. J. Rybicki, D. Mitsouras, A. U. Coskun, and C. L. Feldman, Comput. Phys. Commun. **181**, 624 (2010).
[11] M. Bernaschi, S. Melchionna, S. Succi, M. Fyta, E. Kaxiras, and J. K. Sircar, Comput. Phys. Commun. **180**, 624 (2009).
[12] M. M. Dupin, I. Halliday, and C. M. Care, Phys. Rev. E **73**, 055701(R) (2006).
[13] S. Succi, *The Lattice Boltzmann Equation for Fluid Mechanics and Beyond* (Clarendon Press, Cambridge, MA, 2001).
[14] P. Lallemand and L. S. Luo, Phys. Rev. E **61**, 6546 (2000), and references therein.
[15] X. Y. He and L. S. Luo, J. Stat. Phys. **88**, 927 (1997).
[16] M. M. Dupin, I. Halliday, and C. M. Care, Phil. Trans. Roy. Soc. A **362**, 1775 (2004).
[17] M. M. Dupin, I. Halliday, and C. M. Care, Med. Eng. Phys. **28**, 13 (2006).
[18] T. J. Spencer, I. Halliday, and C. M. Care, Phys. Rev. E **82**, 066701 (2010).
[19] R. Weinstock, *Calculus of Variations with Applications to Physics and Engineering* (McGraw-Hill, New York, 1952).
[20] S. V. Lishchuk, C. M. Care, and I. Halliday, Phys. Rev. E **67**, 036701 (2003).
[21] X. Shan and H. Chen, Phys. Rev. E **49**, 2941 (1994).
[22] A. K. Gunstensen, D. H. Rothman, S. Zaleski, and G. Zanetti, Phys. Rev. A **43**, 4320 (1991).
[23] M. R. Swift, W. R. Osborn, and J. M. Yeomans, Phys. Rev. Lett. **75**, 830 (1995).
[24] M. R. Swift, E. Orlandini, W. R. Osborn, and J. M. Yeomans, Phys. Rev. E **54**, 5041 (1996).
[25] A. J. Wagner, Phys. Rev. E **74**, 056703 (2006)
[26] Q. Li and A. J. Wagner, Phys. Rev. E **76**, 036701 (2007), and references therein.
[27] A. J. Wagner and C. M. Pooley, Rev. E **76**, 056703 (2007), and references therein.
[28] I. Halliday, A. P. Hollis, and C. M. Care, Phys. Rev. E **76**, 026708 (2007).
[29] L. Landau and E. M. Lifshitz, *Fluid Mechanics*, 3rd ed. (Pergammon Press, New York, 1966).
[30] X. He, S. Chen, and G. D. Doolen, J. Comput. Phys. **146**, 282 (1998).
[31] Z. Guo, C. Zheng, and B. Shi, Phys. Rev. E **65**, 046308 (2002).
[32] Y. H. Qian, D. d'Humières, and P. Lallemand, Europhys. Lett. **17**, 479 (1992).
[33] U. D'Ortona, D. Salin, M. Cieplak, R. B. Rybka, and J. R. Banavar, Phys. Rev. E **51**, 3718 (1995).
[34] S. V. Lishchuk, I. Halliday, and C. M. Care, Phys. Rev. E **77**, 036702 (2008).
[35] J. S. Rawlinson and B. Widom, *The Molecular Theory of Capillarity* (Clarendon Press, Cambridge, MA, 1982).
[36] S. Zaleski, J. Li, and S. Succi, Phys. Rev. Lett. **75**, 244 (1995).
[37] J. Feng and S. Weinbaum, J. Fluid Mech. **422**, 281 (2000).
[38] N.-Q. Nguyen and A. J. C. Ladd, Phys. Rev. E **66**, 046708 (2002).
[39] R. Benzi, S. Chibbaro, and S. Succi, Phys. Rev. Lett. **102**, 026002 (2009).